Chapter 5

Dark matter detection rates

Now that the design and optimisation of SABRE South has been discussed in great detail, a question naturally presents itself: how well will the setup be able to observe DM? And, how can this ability be quantified and compared to the capability of other experiments that use different targets?
This Chapter explains in detail the various ingredients required for this calculation, and presents a method used to compute the sensitivity of an experiment to the DM modulation signal designed for use in Refs. [100, 101].
In general, the DM detection rate depends on three key inputs: theoretical explanation of how the interaction process proceeds, the DM velocity distribution, and the detector response to the interaction rate the first two produce. These are discussed separately in the following sections.

5.1 Dark matter interaction rate

The differential DM interaction rate (as in, how frequently an interaction is expected to occur between DM and some target), with respect to nuclear recoil energy E_R, is given by

$$\frac{dR}{dE_R} = N_T \frac{\rho}{m_\chi} \int_{v_{\min}}^{v_{\rm esc}} v f_{lab}(\vec{v}) \frac{d\sigma_T}{dE_R} d^3v, \tag{5.1}$$

where the N_T is the number of target atoms per kg of target, ρ the DM density, $d\sigma_T/dE_R$ the scattering cross section, and $f_{lab}(v)$ is the DM velocity distribution in the lab frame, with an that integral goes from the minimum velocity in the lab frame that can produce a recoil of a given energy,

$$v_{\min} = \sqrt{\frac{m_T E_R}{2\mu_{\chi,T}^2}}, \tag{5.2}$$

up to the galactic escape velocity. The reduced mass of the system, $\mu_{\chi,T}$, is given by

$$\mu_{\chi,T} = \frac{m_\chi m_T}{m_\chi + m_T}. \tag{5.3}$$

Typically, one can interpret the scattering cross section $d\sigma_T/dE_R$ as the particle physics content of the interaction rate, while the velocity distribution $f(v)$ is the astrophysical contribution. The calculations of these will be discussed in the following subsections, before a sensible way to combine them (designed for the analysis of this thesis) is presented.

5.1.1 Dark matter particle interactions

In general, the scattering cross section is computed by taking the squared scattering matrix and averaging it over the spins

$$\frac{d\sigma_T}{dE_R} = \frac{m_T}{2\pi v^2} \left[\frac{1}{2j_\chi + 1} \frac{1}{2j_T + 1} \sum_{\text{spins}} |\mathcal{M}|^2 \right], \tag{5.4}$$

where j_χ and j_T are the spins of the DM and target. The exact expression for $\sum_{\text{spins}} |\mathcal{M}|^2$ will depend on the particular interaction of interest. Typically, this is computed by using an Effective Field theory (EFT) with an effective Hamiltonian constructed from a number of operators $\mathcal{O}_j$ that depend on the exact process of the scattering:

$$\mathcal{H}(\mathbf{r}) = \sum_{\tau=0,1} \sum_{j=1}^{15} c_j^\tau \mathcal{O}_j(\mathbf{r}) t^\tau, \tag{5.5}$$

where $t^0 = \mathbb{1}$ and $t^1 = \sigma_3$, the third Pauli matrix. The exact interaction that occurs between DM and a nucleus is described by the non-relativistic nucleon operators $\mathcal{O}_i$ for a particular model. Each of these operators will correspond to an effective high energy operator and is the result of integrating out the (unknown) mediator, which dictates the DM model under consideration. In some cases, a non-relativistic nucleon operator may be associated with more than one high energy effective operator, meaning that the two models cannot be distinguished via a direct detection experiment.
These operators depend on a number of different factors, including the exchanged momentum $\vec{q}$, the incoming relative velocity $\vec{v}$, and the DM and nuclear spins $\vec{j}_\chi$ and $\vec{j}_N$. The superscript τ allows for isoscalar ($\tau = 0$) and isovector ($\tau = 1$) couplings, which are related to proton and neutron couplings c_j^p and c_j^n via

$$\begin{aligned} c_j^p &= \frac{1}{2}\left(c_j^0 + c_j^1\right), \\ c_j^n &= \frac{1}{2}\left(c_j^0 - c_j^1\right). \end{aligned} \tag{5.6}$$

Following the methodology of Ref. [102–104], these operators can be used to calculate the cross section for scattering between DM and a nucleus via typical EFT formalism.

The couplings c_j influence the detection rate via the inclusion of the nuclear form factors $F_{ij}^{(ab)}(v, q)$, which convert the scattering cross section of a single nucleon into a cross section that can be used for a full target nucleus. This is then used to represent the scattering matrix;

$$\frac{1}{2j_\chi + 1}\frac{1}{2j_T + 1}\sum_{\text{spins}} |\mathcal{M}|^2 = \sum_{i,j}^{15} \sum_{a,b=0,1} c_i^{(a)} c_j^{(b)} F_{ij}^{(ab)}(v, q), \tag{5.7}$$

where $c_{i,j}$ are the same coefficients of Eq. 5.5, and q is related to E_R by

$$q^2 = 2 m_T E_R. \tag{5.8}$$

Here, and throughout this thesis, N subscripts refer to an individual nucleon while a T refers to the full target nucleus. A full list of the form factors used in this analysis for ^{23}Na and ^{127}I can be found in Appendix A of Ref. [102].
To ease computation, as in Ref. [105], it is possible to express these coupling constants as a vector $\boldsymbol{c_0}$

$$\boldsymbol{c_0} = \sum_{i}^{15} \sum_{a=0,1} \boldsymbol{c}_i^{(a)} \hat{e}_i^a = c_0 \hat{\boldsymbol{c}}_\mathbf{0}, \tag{5.9}$$

where $\hat{e}_i^{(a)}$ are unit vectors that represent the relative coupling strength of the various operators. In this way, the fit of the couplings constants can be separated into the fit of the

direction and norm of the vector $\boldsymbol{c_0}$. Thus, all the information about the relative contributions of different operators/form factors are contained within $\hat{\boldsymbol{c}}_{\mathbf{0}}$, allowing for c_0 to be pulled out of Eq. 5.7 as a common factor:

$$\frac{1}{2j_\chi+1}\frac{1}{2j_T+1}\sum_{\text{spins}}|\mathcal{M}|^2 = c_0^2\sum_{i,j}\sum_{a,b=0,1}\hat{c}_i^{(a)}\hat{c}_j^{(b)}F_{ij}^{(ab)}(v,q). \tag{5.10}$$

Adopting the parameterisation

$$\sigma_\chi \equiv \frac{\mu_N^2 c_0^2}{\pi} \tag{5.11}$$

then allows for fits to a DM cross section σ_χ, as well as m_χ, and the components of $\hat{\boldsymbol{c}}_{\mathbf{0}}$. The differential cross section can this be expressed as

$$\begin{aligned}\frac{d\sigma_T}{dE_R} &= \frac{m_T}{2\pi v^2}\left[\frac{1}{2j_\chi+1}\frac{1}{2j_T+1}\sum_{\text{spins}}|\mathcal{M}|^2\right], \\ &= \frac{m_T}{2v^2}\frac{\sigma_\chi}{\mu_N^2}\left[\sum_{i,j}\sum_{a,b=0,1}\hat{c}_i^{(a)}\hat{c}_j^{(b)}F_{ij}^{(ab)}(v,q)\right].\end{aligned} \tag{5.12}$$

It should be noted, however, that the value of σ_χ, and indeed what it *physically represents* will depend on the basis in which $\boldsymbol{c_0}$ is normalised. For example, with $\boldsymbol{c_0}$ normalised as shown in Eq. 5.9, σ_χ will represent the coupling between DM and the isospin state of the target. To compute the coupling between DM and the nucleus, $\boldsymbol{c_0}$ would need to be normalised with respect to the nuclear basis so that

$$\boldsymbol{c_0} = \sum_{i}^{15}\sum_{a=n,p}\boldsymbol{c}_i^{(a)}\hat{e}_i^a = c_0\hat{\boldsymbol{c}}_{\mathbf{0}}. \tag{5.13}$$

Alternatively, the direct coupling between DM and a particular nucleon can also be found using the conversions in Eq. 5.6. To avoid confusion, the rest of this thesis will use the following notation to distinguish between the slightly different forms and meanings of σ_χ

- $\sigma_{\chi,0}$ - the scattering cross section for DM off the isospin state of a nucleus.
- $\sigma_{\chi,N}$ - the scattering cross section for DM off an atomic nucleus.
- $\sigma_{\chi,p}$ - the scattering cross section for DM off a proton (or neutron, where n is used instead of p).

Nominally, any one of these can be used to calculate the other two but, where possible, results will be presented for $\sigma_{\chi,p}$ as tends to be standard for the literature.

5.1.2 Dark matter velocity distributions

As discussed in Chapter 1, the velocity distribution typically assumed for galactic DM is the Standard Halo Model (SHM), where the DM follows a Maxwell Boltzmann distribution

$$f_{\text{SHM}}(v) = \frac{1}{(\pi v_0^2)^{3/2}}\exp\left[-\frac{1}{v_0^2}\left(\vec{v}+\vec{v}_E\right)^2\right]. \tag{5.14}$$

The velocity of the Earth is given by $\vec{v}_E = \vec{v}_\odot + \vec{v}_t$, where

$$\begin{aligned} \vec{v}_\odot &= v_\odot(0,0,1), \\ \vec{v}_t &= v_t(\sin 2\pi t, \sin\gamma\cos 2\pi t, \cos\gamma\cos 2\pi t). \end{aligned} \tag{5.15}$$

In this frame of reference, the DM velocity is expressed as $\vec{v} = v(\sin\theta\cos\phi, \sin\theta\sin\phi, \cos\theta)$. The typically assumed values for constants are given in Table 5.1.

DM density	ρ	0.3 GeV cm^{-3}
Dispersion velocity	v_0	220 km/s
Escape speed	v_{esc}	550 km/s
Solar	$v_\odot$	232 km/s
Rotational velocity	v_t	30 km/s
Angle of orbit	γ	$\pi/3$ km/s

Table 5.1: Typical values used for particular velocity distributions.

As discussed in detail in Sec. 1.3.1, the relative motion of the Earth around the Sun as it moves through the galactic WIMP flux produces an annual modulation, the value of which will depend on the value of $v_{\rm min}$. As shown in Eq. 5.2, $v_{\rm min}$ will change with both target and DM masses, meaning that the same DM particle can and will produce very different looking modulation amplitudes in different experiments. In particular, combinations that give $v_{\rm min}<$ 200 km/s will generate a *negative* modulation that peaks in December rather than the traditionally expected June. To get a basic understanding of how much this $v_{\rm min}$ will impact the modulation fraction, the integral of the velocity distribution in January is subtracted from the integral in June, and divided by the average velocity. This is plotted as a function of $v_{\rm min}$in Fig. 5.1 and gives modulation fractions that range from -2.5% up to 30% for the SHM model. Although the value of this modulation fraction is typically quoted as on the order of 1% [106], it is clear from these plots that this can vary depending on the target, and change even more for interaction models like those detailed in Ref. [107] (and discussed in Sec. 6.1) that increase the minimum velocity accessible by a target. Thus, although this modulation is a useful signpost for searches, analysis of a clear R_0 attributable to DM as well as R_m is required to distinguish between various models under consideration.

As well as the dependence on $v_{\rm min}$, results from the *Gaia* satellite and astrophysical simulations have suggested that the SHM is too simplistic to describe the DM content of the Milky Way [108–110]. In particular it is becoming increasingly accepted that the DM distribution is likely to have substructure that mimics that observed in baryonic matter, such as the Helmi [111] or Sequoia [112] streams and the Gaia Enceladus (GSE) [113]. The exact nature of the substructure will impact the expected interaction rate in different ways. First, it will impact the annual modulation as not all the substructure is aligned with the usual 'WIMP wind', meaning that the interaction rate will no longer produce a nice clean cosine. Second, although the distribution $f_{\rm lab}(v)$ itself is independent of both the interaction model and target under consideration, the integral bound $v_{\rm min}$ will be influenced by both the DM and target masses. Thus, substructure that appears in either the low or high velocity regions can mean that different targets can observe significantly different interaction rates for the same model.

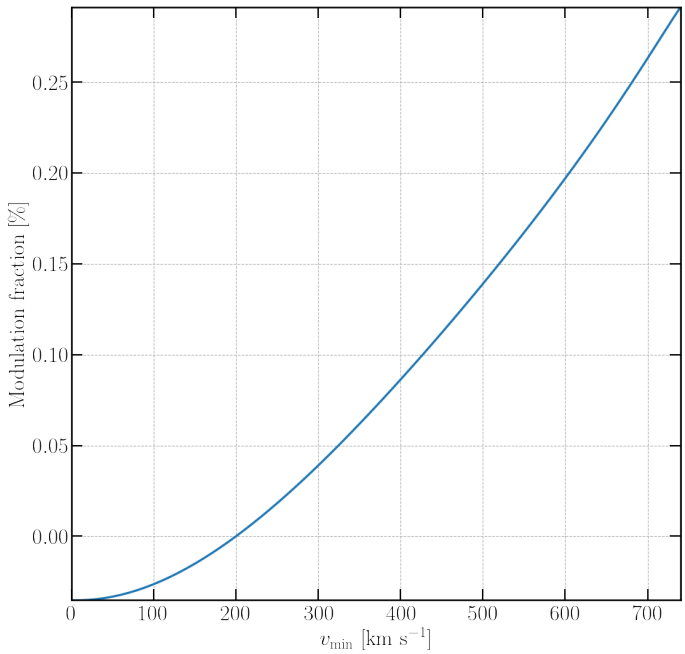

Figure 5.1: Integral of the velocity distribution in June minus the distribution in January as a function of minimum velocity, divided by the average velocity to give the modulation fraction.

Substructure is typically added to the velocity distribution by introducing a substructure scaling factor η so

$$f(v) = (1-\eta) f_{\text{SHM}}(v) + \eta f_{\text{sub}}(v), \tag{5.16}$$

where $f_{\text{sub}}(v)$ describes the substructure being included, and η is able to take values up to 0.3.
Much like the modulation fraction itself, features induced by these substructures will change from detector to detector, and so in an ideal case results across a variety of different targets would be used to constrain the correct distribution. A few examples of these, and their impact on interpreting data, are explored further in Sec. 6.6.1.

5.1.3 Total interaction rate

To allow for easier computation by separating the particle theory and astrophysics contributions, the observation is made that all the terms in the form factor sum are either independent of velocity, or proportional to v^2. This allows for the separation of form factors so

$$F_{ij}^{(ab)}(v,q) = F_{ij}^{(ab),1}(q) + v^2 F_{ij}^{(ab),2}(q). \tag{5.17}$$

Therefore, the cross section can be expressed as two terms, with different velocity dependence:

$$\begin{aligned} \frac{d\sigma_T}{dE_R} &= \frac{1}{v^2}\left(\frac{d\sigma_T^1}{dE_R} + v^2 \frac{d\sigma_T^2}{dE_R}\right), \text{ where} \\ \frac{d\sigma_T^l}{dE_R} &= \frac{m_T}{2}\frac{\sigma_0}{\mu_N^2}\left[\sum_{i,j}\sum_{a,b=0,1} \hat{c}_i^{(a)} \hat{c}_j^{(b)} F_{ij}^{(ab),l}(q)\right]. \end{aligned} \tag{5.18}$$

Using this, Eq. 5.1 can be rewritten in terms of two integrals:

$$\frac{dR}{dE_R} = N_T \frac{\rho}{m_\chi} \frac{\sigma_0 m_T}{2\mu_N^2} \sum_{i,j} \sum_{a,b=0,1} \hat{c}_i^{(a)} \hat{c}_j^{(b)} \left(F_{ij}^{(ab),1}(q) \int \frac{f_{\rm lab}(\vec{v})}{v} d^3v + F_{ij}^{(ab),2}(q) \int v f_{\rm lab}(\vec{v}) d^3v \right). \tag{5.19}$$

To simplify this, the velocity integrals are expressed as

$$\begin{aligned} \int \frac{f_{\rm lab}(\vec{v})}{v} d^3v &= g(v_{\rm min}) = \iint_{\mathcal{D}} v \; f_{\rm lab}(\vec{v}) dv \; d\Omega, \\ \int v f_{\rm lab}(\vec{v}) d^3v &= h(v_{\rm min}) = \iint_{\mathcal{D}} v^3 \; f_{\rm lab}(\vec{v}) dv \; d\Omega. \end{aligned} \tag{5.20}$$

with $\mathcal{D}$ defined as

$$v > v_{\rm min}(E_R), \quad |\vec{v} + \vec{v}_E| < v_{\rm esc}. \tag{5.21}$$

These integrals then form prefactors that, aside from $v_{\rm min}$, do not depend on the particle physics DM model in question. They are then multiplied by the appropriate form factors, giving

$$\begin{aligned} \frac{dR}{dE_R} &= N_T \frac{\rho}{m_\chi} \left[\frac{d\sigma_1}{dE_R} g(v_{\rm min}) + \frac{d\sigma_2}{dE_R} h(v_{\rm min}) \right] \\ &= N_T \frac{\rho}{m_\chi} \frac{\sigma_0 m_T}{2\mu_N^2} \sum_{i,j} \sum_{a,b=0,1} \hat{c}_i^{(a)} \hat{c}_j^{(b)} \left[F_{ij}^{(ab),1}(q) g(v_{\rm min}) + F_{ij}^{(ab),2}(q) h(v_{\rm min}) \right]. \end{aligned} \tag{5.22}$$

The benefit of expressing the rate in this way is that it allows for the separate calculation of the astro and particle physics contributions. This makes computation and comparison for different combinations of DM interaction models and velocity distributions significantly easier to perform, as it removes the need to reevaluate these integrals for every different DM model. Where an explicit expression for the modulation is desired, expressions in Eq. 5.20 can be projected onto $A + B\cos[\omega(t - t_0)]$, giving an interaction rate of the form

$$\frac{dR(t)}{dE_R} = \frac{dR_0}{dE_R} + \frac{dR_m}{dE_R} \cos[\omega(t - t_0)]. \tag{5.23}$$

As such, there are four forms for the velocity distribution that are of use for these calculations: $g_0(v_{\rm min})$, $g_m(v_{\rm min})$, $h_0(v_{\rm min})$, and $h_m(v_{\rm min})$. These are shown for the SHM in Fig. 5.2.

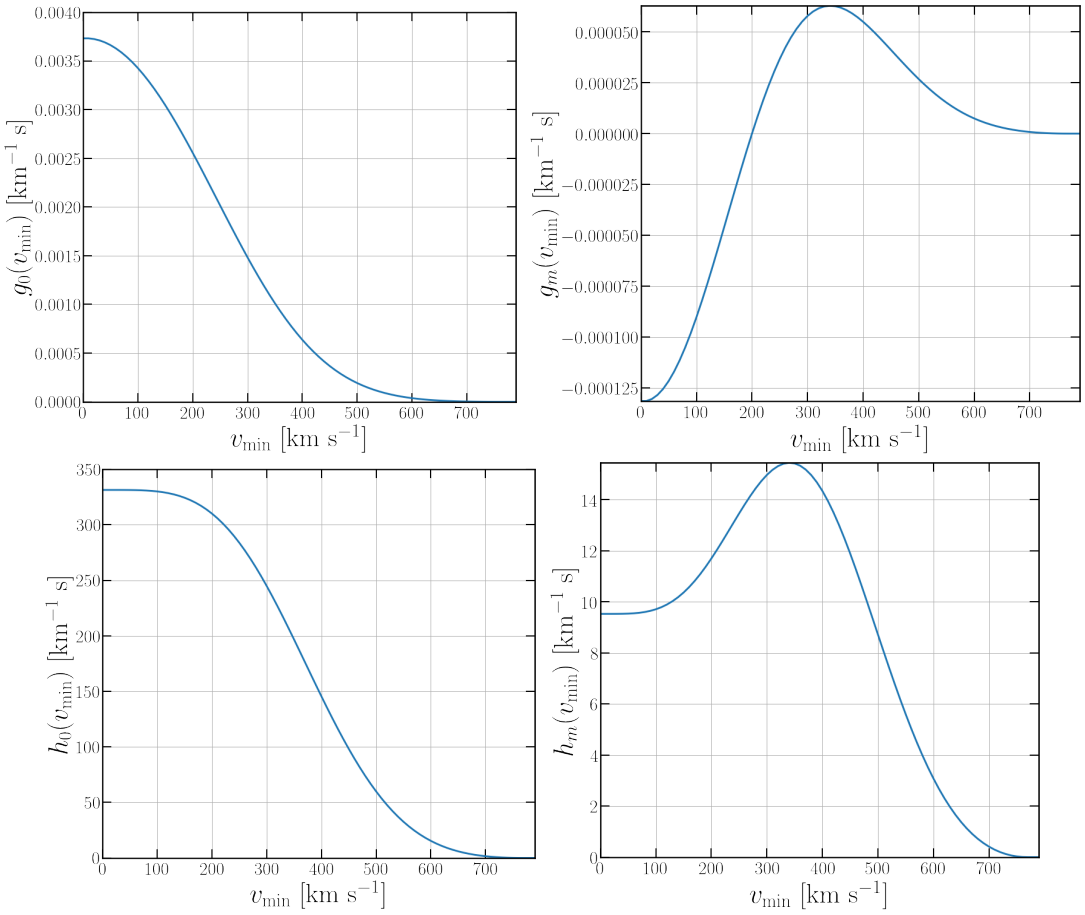

Figure 5.2: Results from the SHM velocity integrals as a function of $v_{\min}$; $g(v_{\min})$ and $h(v_{\min})$, where the modulating and constant components have been separated.

5.2 Detector response

The expression given in Eq. 5.1 is the expected rate of nuclear recoils due to DM. In reality, the detection process will introduce additional threshold cutoffs, smearing, and require calibration between the actual nuclear recoil energy, and the energy measured by the detector. Thus the observation rate (referred to here and the rest of this thesis as dR/dE') as a function of the observed energy (E' in units of keV$_{\text{ee}}$) will take a different form to that of the interaction rate (dR/dE_R) as a function of the nuclear recoil energy (E_R in units of keV$_{\text{NR}}$).

5.2.1 Quenching factors

For scintillation detectors, the intrinsic light yield of the target can be different for electron vs. nuclear recoils [114, 115]. Because these setups tend to be calibrated with gamma ray sources, energy depositions are recorded in units of electron equivalent keV (keV$_{\text{ee}}$), which is based on the amount of light that an electron recoil of that value would produce. To model nuclear recoils (which are the expected signal for DM), a calibration known as the quenching factor (QF) must be used. Essentially, it is a unit conversion between the observed electron equivalent energy E_{ee} (keV$_{\text{ee}}$) and the actual nuclear recoil energy E_R (keV$_{\text{NR}}$), and can be

computed using neutron scattering experiments. This correction takes the form

$$\begin{aligned} E_R &= \frac{E_{\text{ee}}}{QF}, \\ \frac{dR}{dE_{\text{ee}}} &= \frac{dR}{dE_R}\frac{dE_R}{dE_{\text{ee}}}. \end{aligned} \tag{5.24}$$

As NaI(Tl) is a composite target, the QF for both Na and I must be measured. In the past, DAMA have made the assumption that for Na, QF=0.3, and for I, QF=0.09 [45]. However, recent studies [114, 116–120] have indicated that for Na in particular this ratio may have some energy and/or detector dependence. As this value relates to the energy region being probed by a detector, it is imperative that it is well understood to ensure the correct DM models and parameters are being constrained or 'discovered'. A selection of measured values are shown in Table 5.2, with a larger range of observations in Fig. 5.3.

Stiegler et al. (2017) [118]		Xu et al. (2015) [117]		Bignell et al. (2021) [116]		Joo et al. (2019) [114]	
E_R (keV$_{\text{NR}}$)	QF (%)	E_R (keV$_{\text{NR}}$)	QF (%)	E_R (keV$_{\text{NR}}$)	QF (%)	E_R (keV$_{\text{NR}}$)	QF (%)
7.31	8.0	5.7 ± 0.7	13.3 ± 1.8	36 ± 5	16.0 ± 1.3	8.7 ± 1.3	9.6 ± 1.6
8.39	5.6	8.8 ± 1.2	12.9 ± 1.4	58 ± 1	19.8 ± 0.9	14.8 ± 1.6	11.3 ± 1.2
9.46	6.8	9.1 ± 1.2	16.2 ± 1.2	65 ± 8	21.0 ± 0.8	22.7 ± 2.0	14.1 ± 1.3
11.6	8.0	14.3 ± 2.4	15.9 ± 1.9	71 ± 10	23.5 ± 0.8	30.1 ± 2.2	17.2 ± 1.3
17.7	10.5	15.0 ± 1.4	16.0 ± 1.0	79 ± 3	21.6 ± 1.1	46.1 ± 2.8	17.3 ± 1.1
20.8	12.5	19.4 ± 1.6	16.8 ± 0.9	86 ± 12	19.4 ± 0.7	62.6 ± 3.2	18.1 ± 0.9
30.2	14.25	24.9 ± 2.4	17.1 ± 1.0	96 ± 3	22.3 ± 0.9	78.9 ± 3.6	21.3 ± 1.0
3104	15.25	29.0 ± 1.9	18.8 ± 0.8			102.7 ± 4.1	22.1 ± 0.9
34.4	14.0	33.3 ± 2.8	19.1 ± 1.1			151.6 ± 5.0	22.9 ± 0.8
39.7	18.0	43.0 ± 2.2	20.4 ± 0.8				
47.7	18.0	51.8 ± 2.6	20.7 ± 1.0				

Table 5.2: A range of observed Na QF values.

It is still an open question within the field whether the differences in these observations are due to systematics, different measurement or calibration methods, or whether the QF is a value that changes from crystal to crystal. Because it is the result of particular optical qualities of a crystal, it is possible that its value changes from crystal to crystal. The impact of the uncertainty surrounding this is discussed further in Sec. 6.2.

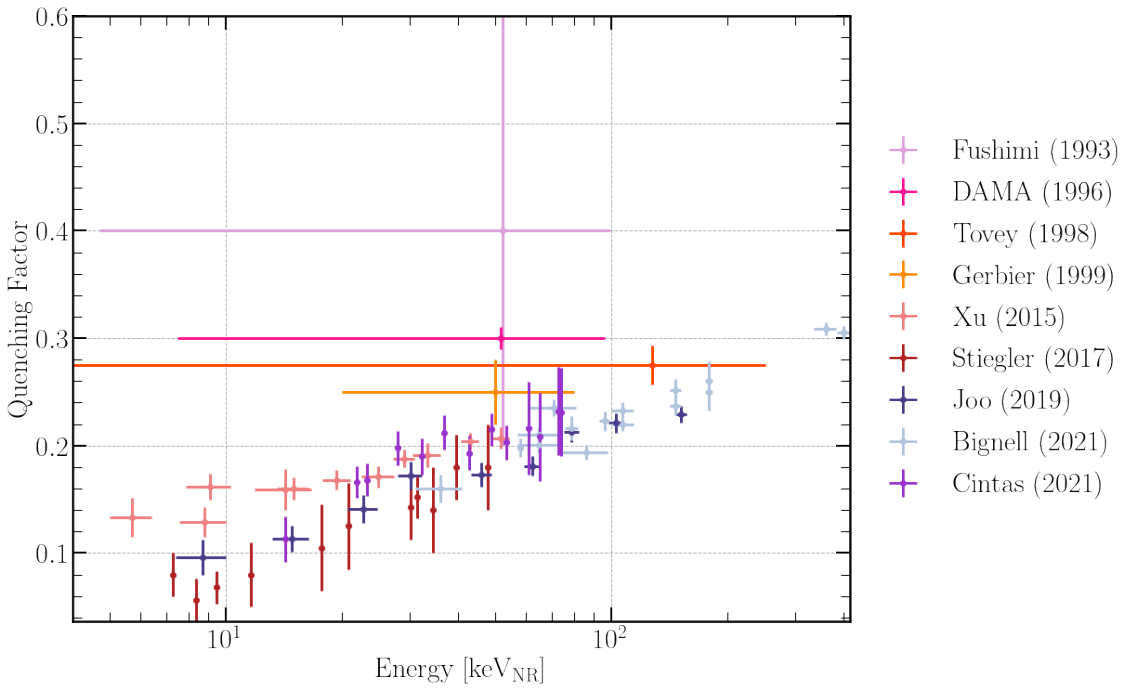

Figure 5.3: A number of Na QF measurements, taken from Refs. [43, 114, 116–122].

5.2.2 Resolution

The energy resolution of a detector is a measurement of how clearly features in the energy spectrum will appear. This will influence the observed rate of interaction, effectively smearing the signal and causing recoils of energy E_{ee} to be observed as a Gaussian distributed spectrum [115]. This can be understood by using a toy signal made up of a series of delta functions. If each delta function is in reality smeared over neighbouring bins, then the total energy rate expected in a particular energy bin E' is the sum of the gaussian contributions from those that neighbour it. Thus, the differential rate will undergo a transformation

$$\frac{dR}{dE'} = \frac{1}{(2\pi)^{1/2}} \int_0^\infty \frac{1}{\Delta E_{\mathrm{ee}}} \frac{dR}{dE_{\mathrm{ee}}} \exp\left[\frac{-(E' - E_{\mathrm{ee}})^2}{2(\Delta E_{\mathrm{ee}})^2}\right] dE_{\mathrm{ee}}, \tag{5.25}$$

where ΔE_{ee} is the energy resolution of the detector. ΔE_{ee} is related to the FWHM of a measured peak in the detector, where ΔE_{ee} =FWHM/2.35 [115]. NaI(Tl) targets tend to use the 59.5 keV$_{\mathrm{ee}}$ peak from ^{214}Am to measure this value.
In general, the resolution of a detector is expected to follow a function of the form

$$\Delta E_{\mathrm{ee}} = \alpha\sqrt{E} + \beta E, \tag{5.26}$$

due to the different sources of fluctuation in the detector. These can be due to a number of features, including drift of detector characteristics over time, random noise, and statistical fluctuations. The factor α can be thought of as the (irreducible) statistics based component, while β accounts for all other sources [96]. For NaI(Tl) detectors, the α term tends to dominate this expression.

5.2.3 Efficiency

The threshold detection efficiency will influence the probability of an event of a given energy actually being observed by the detector. This will depend on a variety of factors, some intrinsic to the detector (such as the quantum efficiency of PMTs) and others that come about due to analysis, e.g., background or veto cuts for a detector. In general it is accounted for by using an energy dependent scale factor $\epsilon(E')$. For the NaI(Tl) experiments of interest for this thesis, the poor low energy efficiency of the detectors constrains their observations to above 1 keV_{ee}.

5.2.4 Total observation rate

Combining these three detector responses, the observation rate as a function of observable energy is

$$\frac{dR}{dE'} = \frac{\epsilon(E')}{(2\pi)^{1/2}} \int_0^\infty \frac{1}{\Delta E_{\text{ee}}} \frac{dR}{dE_R} \frac{dE_R}{dE_{\text{ee}}} \exp\left[\frac{-(E' - E_{\text{ee}})^2}{2(\Delta E_{\text{ee}})^2}\right] dE_{\text{ee}}. \tag{5.27}$$

Here, all of the model dependent terms are contained within $\frac{dR}{dE_R}$. The general workflow of such a computation (developed in Ref. [123] for this thesis) is shown in Fig. 5.4. This was designed to be modular in form, to allow for easy implementation of improved astrophysical or theoretical calculations, and to easily test different experimental variables.

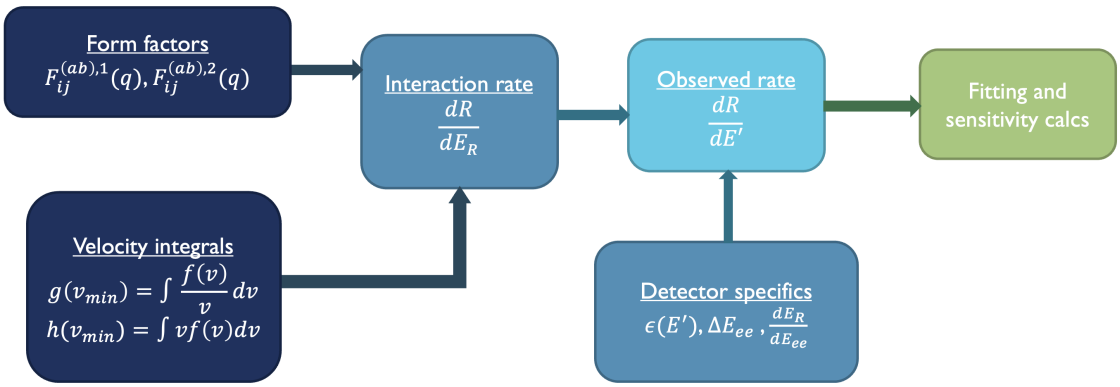

Figure 5.4: DM computation workflow, implemented in Ref. [123].

5.2.5 Multi element targets

For DM targets that are made up of more than one element, such as NaI, the calculations for each element must be done separately, then added together. Thus the total, overall rate will be given by the rate in each target nucleus i, weighted by their contributing masses m_i as a fraction of the total molecular mass m_{Tot}:

$$\frac{dR_{\text{Tot}}}{dE'} = \sum_i \frac{m_i}{m_{\text{Tot}}} \frac{dR_i}{dE'}. \tag{5.28}$$

For NaI(Tl) detectors, the two DM targets are the Na and I (the Tl is present in low levels only to support the scintillation process), and so the total DM rate will be

$$\frac{dR_{\text{Tot}}}{dE'} = \frac{m_{\text{Na}}}{m_{\text{Na}} + m_{\text{I}}} \frac{dR_{\text{Na}}}{dE'} + \frac{m_{\text{I}}}{m_{\text{Na}} + m_{\text{I}}} \frac{dR_I}{dE'}. \tag{5.29}$$

5.3 Experimental sensitivity

In general, experimental sensitivity is assessed based on how well a signal can be distinguished over some background model. For frequentist statistics, this can be thought of as hypothesis tests, and will fall into one of two categories:

1. Signal discovery: the background only model is adopted as the null hypothesis, and tested against the alternative hypothesis of background plus the signal of interest.

2. Signal exclusion: the signal plus background model is adopted as the null hypothesis, and tested against the alternative of the background only case.

These are used to quantify experimental sensitivity by simulating or generating data under the alternative hypothesis, and testing its compatibility with the predictions of the null hypothesis [124]. This is done by constructing probability distribution functions (PDFs) for both the background only and signal+background hypothesis, that demonstrate the relative probability of observing some value under the assumption of that model. Experimental sensitivity (based on simulation) is concerned with the median significance with which a model can be rejected, rather than a single data set (which would be collected once an experiment is operational). In order to do this, the median value for the alternative hypothesis should be used to test the null hypothesis, where the sensitivity can be characterised by the p-value of this median value [124]. This is illustrated in Fig. 5.5.
In this context, the discovery power of an experiment can be thought of as the probability of observing data compatible with the signal+background hypothesis if the background only model is true (a detector has seen a 'signal' - is it just background?), and the exclusion power the probability of observing data compatible with the background only hypothesis if the signal+background model is true (a detector has seen 'nothing' - is the signal just too small?).

For experiments like SABRE that aim to explicitly test the modulation of a DM signal, the key background of concern is the apparent modulation of a (presumably) constant rate due to statistical fluctuations, as analysis of the modulation signature typically involves the subtraction of the constant signal component, or fitting to some cosine function [37]. As such, to construct the PDFs used to test experimental sensitivity, these fluctuations should be modelled over a detector's lifetime, and fit to a cosine function to find the probability distribution for observable modulation under both hypotheses.

References

[1] R. Bernabei et al. "First model independent results from DAMA/LIBRA-phase2". In: (2018), pp. 1–28. arXiv: 1805.10486. URL: http://arxiv.org/abs/1805.10486.

[2] M. Tanabashi et al. "Review of Particle Physics". In: *Phys. Rev. D* 98 (3 Aug. 2018), p. 030001. DOI: 10.1103/PhysRevD.98.030001. URL: https://link.aps.org/doi/10.1103/PhysRevD.98.030001.

[3] G. Arnison et al. "Experimental Observation of Isolated Large Transverse Energy Electrons with Associated Missing Energy at $\sqrt{s} = 540$ GeV". In: *Phys. Lett. B* 122 (1983), pp. 103–116. DOI: 10.1016/0370-2693(83)91177-2.

[4] G. Arnison et al. "Experimental Observation of Lepton Pairs of Invariant Mass Around 95-GeV/c**2 at the CERN SPS Collider". In: *Phys. Lett. B* 126 (1983), pp. 398–410. DOI: 10.1016/0370-2693(83)90188-0.

[5] Claudio Campagnari and Melissa Franklin. "The Discovery of the top quark". In: *Rev. Mod. Phys.* 69 (1997), pp. 137–212. DOI: 10.1103/RevModPhys.69.137. arXiv: hep-ex/9608003.

[6] Serguei Chatrchyan et al. "Observation of a New Boson at a Mass of 125 GeV with the CMS Experiment at the LHC". In: *Phys. Lett. B* 716 (2012), pp. 30–61. DOI: 10.1016/j.physletb.2012.08.021. arXiv: 1207.7235 [hep-ex].

[7] Georges Aad et al. "Observation of a new particle in the search for the Standard Model Higgs boson with the ATLAS detector at the LHC". In: *Phys. Lett. B* 716 (2012), pp. 1–29. DOI: 10.1016/j.physletb.2012.08.020. arXiv: 1207.7214 [hep-ex].

[8] Steven Weinberg. "The U(1) Problem". In: *Phys. Rev. D* 11 (1975), pp. 3583–3593. DOI: 10.1103/PhysRevD.11.3583.

[9] Y. Fukuda et al. "Evidence for oscillation of atmospheric neutrinos". In: *Phys. Rev. Lett.* 81 (1998), pp. 1562–1567. DOI: 10.1103/PhysRevLett.81.1562. arXiv: hep-ex/9807003.

[10] Planck Collaboration et al. "Planck 2018 results. VI. Cosmological parameters". In: (July 2018). arXiv: 1807.06209. URL: http://arxiv.org/abs/1807.06209.

[11] Vera C. Rubin and W. Kent Ford Jr. "Rotation of the Andromeda Nebula from a Spectroscopic Survey of Emission Regions". In: *Astrophys. J.* 159 (1970), pp. 379–403. DOI: 10.1086/150317.

[12] Katherine Freese. "Review of Observational Evidence for Dark Matter in the Universe and in upcoming searches for Dark Stars". In: (Dec. 2008). DOI: 10.1051/eas/0936016. arXiv: 0812.4005. URL: https://arxiv.org/abs/0812.4005.

[13] J. K. Adelman-McCarthy et al. "The Fourth Data Release of the Sloan Digital Sky Survey". In: (July 2005). DOI: 10.1086/497917. arXiv: 0507711 [astro-ph]. URL: https://arxiv.org/abs/astro-ph/0507711.

[14] Douglas Clowe et al. "A Direct Empirical Proof of the Existence of Dark Matter". In: *The Astrophysical Journal* 648.2 (Aug. 2006), pp. L109–L113. DOI: 10.1086/508162. URL: https://doi.org/10.1086/508162.

[15] Marc Davis et al. "The Evolution of Large Scale Structure in a Universe Dominated by Cold Dark Matter". In: *Astrophys. J.* 292 (1985). Ed. by M. A. Srednicki, pp. 371–394. DOI: 10.1086/163168.

[16] Katherine Garrett and Gintaras Duda. "Dark Matter: A Primer". In: *Advances in Astronomy* 2011 (2011), pp. 1–22. DOI: 10.1155/2011/968283. URL: https://doi.org/10.1155%5C%2F2011%5C%2F968283.

[17] Gerard Jungman, Marc Kamionkowski, and Kim Griest. "Supersymmetric dark matter". In: *Phys. Rept.* 267 (1996), pp. 195–373. DOI: 10.1016/0370-1573(95)00058-5. arXiv: hep-ph/9506380.

[18] T. M. P. Tait. *Complementarity of Dark Matter Searches*. Lepton Photon. June 2013.

[19] Bobby Samir Acharya et al. "A Non-thermal WIMP Miracle". In: *Phys. Rev. D* 80 (2009), p. 083529. DOI: 10.1103/PhysRevD.80.083529. arXiv: 0908.2430 [astro-ph.CO].

[20] R. Khatiwada et al. "Axion Dark Matter Experiment: Detailed design and operations". In: *Review of Scientific Instruments* 92.12 (Dec. 2021), p. 124502. DOI: 10.1063/5.0037857. URL: https://doi.org/10.1063%5C%2F5.0037857.

[21] Aaron Quiskamp et al. "Direct search for dark matter axions excluding ALP cogenesis in the 63- to 67-μeV range with the ORGAN experiment". In: *Science Advances* 8.27 (July 2022). DOI: 10.1126/sciadv.abq3765. URL: https://doi.org/10.1126%5C%2Fsciadv.abq3765.

[22] ATLAS Collaboration. *Constraints on spin-0 dark matter mediators and invisible Higgs decays using ATLAS 13 TeV pp collision data with two top quarks and missing transverse momentum in the final state*. 2022. DOI: 10.48550/ARXIV.2211.05426. URL: https://arxiv.org/abs/2211.05426.

[23] Rebecca K. Leane et al. *Snowmass2021 Cosmic Frontier White Paper: Puzzling Excesses in Dark Matter Searches and How to Resolve Them*. 2022. DOI: 10.48550/ARXIV.2203.06859. URL: https://arxiv.org/abs/2203.06859.

[24] Rouven Essig et al. *Snowmass2021 Cosmic Frontier: The landscape of low-threshold dark matter direct detection in the next decade*. 2022. DOI: 10.48550/ARXIV.2203.08297. URL: https://arxiv.org/abs/2203.08297.

[25] E. Aprile et al. "An approximate likelihood for nuclear recoil searches with XENON1T data". In: *Eur. Phys. J. C* 82.11 (2022), p. 989. DOI: 10.1140/epjc/s10052-022-10913-w. arXiv: 2210.07231 [hep-ex].

[26] J. Aalbers et al. "First Dark Matter Search Results from the LUX-ZEPLIN (LZ) Experiment". In: (July 2022). arXiv: 2207.03764 [hep-ex].

[27] Kevin Thieme. "DARWIN a next-generation liquid xenon observatory for dark matter and neutrino physics". In: *PoS* ICRC2021 (2021), p. 548. DOI: 10.22323/1.395.0548.

[28] M. F. Albakry et al. "A Strategy for Low-Mass Dark Matter Searches with Cryogenic Detectors in the SuperCDMS SNOLAB Facility". In: *2022 Snowmass Summer Study*. Mar. 2022. arXiv: 2203.08463 [physics.ins-det].

[29] G. Angloher et al. "Limits on Dark Matter Effective Field Theory Parameters with CRESST-II". In: *Eur. Phys. J. C* 79.1 (2019), p. 43. DOI: 10.1140/epjc/s10052-018-6523-4. arXiv: 1809.03753 [hep-ph].

[30] H. Lattaud. "Sub-GeV Dark Matter Searches with EDELWEISS: New results and prospects". In: *14th International Workshop on the Identification of Dark Matter 2022*. Nov. 2022. arXiv: 2211.04176 [astro-ph.GA].

[31] Ciaran A. J. O'Hare. "New Definition of the Neutrino Floor for Direct Dark Matter Searches". In: *Physical Review Letters* 127.25 (Dec. 2021). DOI: 10.1103/physrevlett.

127.251802. URL: https://doi.org/10.1103%5C%2Fphysrevlett.127.251802.

[32] Masahiro Ibe et al. "Migdal effect in dark matter direct detection experiments". In: *JHEP03* (2018), p. 194. DOI: 10.1007/JHEP03(2018)194. URL: https://doi.org/10.1007/JHEP03.

[33] Matthew J. Dolan, Felix Kahlhoefer, and Christopher McCabe. "Directly detecting sub-GeV dark matter with electrons from nuclear scattering". In: (Nov. 2017). DOI: 10.1103/PhysRevLett.121.101801. arXiv: 1711.09906.

[34] Simon Knapen, Tongyan Lin, and Kathryn M. Zurek. "Light dark matter in superfluid helium: Detection with multi-excitation production". In: *Physical Review D* 95.5 (Mar. 2017). DOI: 10.1103/physrevd.95.056019. URL: https://doi.org/10.1103%5C%2Fphysrevd.95.056019.

[35] Yonit Hochberg et al. "Detection of sub-MeV dark matter with three-dimensional Dirac materials". In: *Physical Review D* 97.1 (Jan. 2018). DOI: 10.1103/physrevd.97.015004. URL: https://doi.org/10.1103%5C%2Fphysrevd.97.015004.

[36] D. S. Akerib et al. *Snowmass2021 Cosmic Frontier Dark Matter Direct Detection to the Neutrino Fog*. 2022. DOI: 10.48550/ARXIV.2203.08084. URL: https://arxiv.org/abs/2203.08084.

[37] R. Bernabei et al. *The dark matter: DAMA/LIBRA and its perspectives*. 2021. arXiv: 2110.04734 [hep-ph].

[38] Stefano Scopel, Kook-Hyun Yoon, and Jong-Hyun Yoon. "Generalized spin-dependent WIMP-nucleus interactions and the DAMA modulation effect". In: *JCAP* 1507.07 (2015), p. 041. DOI: 10.1088/1475-7516/2015/07/041. arXiv: 1505.01926 [astro-ph.CO].

[39] J Amaré et al. "Analysis of backgrounds for the ANAIS-112 dark matter experiment". In: *Eur. Phys. J. C* 79 (2019), p. 412. DOI: 10.1140/epjc/s10052-019-6911-4.

[40] M Antonello et al. *The SABRE project and the SABRE Proof-of-Principle*. Tech. rep. 2018. arXiv: 1806.09340v2.

[41] G. Adhikari et al. *Three-year annual modulation search with COSINE-100*. 2021. arXiv: 2111.08863 [hep-ex].

[42] F Reindl et al. "Results of the first NaI scintillating calorimeter prototypes by COSINUS". In: *Journal of Physics: Conference Series* 1342.1 (Jan. 2020), p. 012099. DOI: 10.1088/1742-6596/1342/1/012099. URL: https://doi.org/10.1088%5C%2F1742-6596%5C%2F1342%5C%2F1%5C%2F012099.

[43] K. Fushimi et al. "Application of a large-volume NaI scintillator to search for dark matter". In: *Phys. Rev. C* 47 (2 Feb. 1993), R425–R428. DOI: 10.1103/PhysRevC.47.R425. URL: https://link.aps.org/doi/10.1103/PhysRevC.47.R425.

[44] A. Bottino et al. "Search for neutralino dark matter with NaI detectors". In: *Physics Letters B* 295.3 (1992), pp. 330–336. ISSN: 0370-2693. DOI: https://doi.org/10.1016/0370-2693(92)91575-T. URL: https://www.sciencedirect.com/science/article/pii/037026939291575T.

[45] R. Bernabei et al. "New limits on WIMP search with large-mass low-radioactivity NaI(Tl) set-up at Gran Sasso". In: *Phys. Lett. B* 389 (1996), pp. 757–766. DOI: 10.1016/S0370-2693(96)01483-9.

[46] R. Bernabei et al. "The DAMA/LIBRA apparatus". In: *Nucl. Instruments Methods Phys. Res. Sect. A Accel. Spectrometers, Detect. Assoc. Equip.* 592.3 (July 2008), pp. 297–315. ISSN: 01689002. DOI: 10.1016/j.nima.2008.04.082.

[47] R. Bernabei et al. "The DAMA project: Achievements, implications and perspectives". In: *Progress in Particle and Nuclear Physics* 114 (2020), p. 103810. ISSN: 0146-6410. DOI: https://doi.org/10.1016/j.ppnp.2020.103810. URL: https://www.sciencedirect.com/science/article/pii/S0146641020300570.

[48] G. Adhikari et al. "The COSINE-100 liquid scintillator veto system". In: *Nuclear Instruments and Methods in Physics Research Section A: Accelerators, Spectrometers, Detectors and Associated Equipment* 1006 (2021), p. 165431. ISSN: 0168-9002. DOI: https://doi.org/10.1016/j.nima.2021.165431.

[49] J. Amaré et al. "Annual modulation results from three-year exposure of ANAIS-112". In: *Phys. Rev. D* 103 (10 May 2021), p. 102005. DOI: 10.1103/PhysRevD.103.102005. URL: https://link.aps.org/doi/10.1103/PhysRevD.103.102005.

[50] B. Suerfu. "SDeveloping Ultra Low-Background Sodium-Iodide Crystal Detector for Dark Matter Searches". PhD thesis. Department of Physics, Princeton University, 2018.

[51] Donald C. Stockbarger. "The Production of Large Single Crystals of Lithium Fluoride". In: *Review of Scientific Instruments* 7.3 (Mar. 1936), pp. 133–136. DOI: 10.1063/1.1752094.

[52] Y. Zhu et al. *Production of ultra-low radioactivity NaI(Tl) crystals for Dark Matter detectors*. 2019. DOI: 10.48550/ARXIV.1909.11692. URL: https://arxiv.org/abs/1909.11692.

[53] Jiayue Xu, Shiji Fan, and Baoliang Lu. "Growth of ∅4 Li2B4O7 single crystals by multi-crucible Bridgman method". In: *Journal of Crystal Growth* 264.1 (2004), pp. 260–265. ISSN: 0022-0248. DOI: https://doi.org/10.1016/j.jcrysgro.2003.12.040. URL: https://www.sciencedirect.com/science/article/pii/S0022024803022395.

[54] R. Bernabei et al. "Performances of the new high quantum efficiency PMTs in DAMA/LIBRA". In: *Journal of Instrumentation* 7.03 (Mar. 2012), P03009–P03009. DOI: 10.1088/1748-0221/7/03/p03009.

[55] G. Adhikari et al. "Initial performance of the COSINE-100 experiment". In: *The European Physical Journal C* 78.2 (Feb. 2018). DOI: 10.1140/epjc/s10052-018-5590-x. URL: https://doi.org/10.1140%5C%2Fepjc%5C%2Fs10052-018-5590-x.

[56] P Adhikari et al. *Background model for the NaI(Tl) crystals in COSINE-100*. Tech. rep. arXiv: 1804.05167v3.

[57] J. Amaré et al. "Performance of ANAIS-112 experiment after the first year of data taking". In: *The European Physical Journal C* 79.3 (Mar. 2019). DOI: 10.1140/epjc/s10052-019-6697-4. URL: https://doi.org/10.1140%5C%2Fepjc%5C%2Fs10052-019-6697-4.

[58] M. Antonello et al. "Characterization of SABRE crystal NaI-33 with direct underground counting". In: *The European Physical Journal C* 81.4 (Apr. 2021). ISSN: 1434-6052. URL: https://doi.org/10.1140/epjc/s10052-021-09098-5.

[59] F. Calaprice et al. *Performance of a SABRE detector module without an external veto*. 2022. DOI: 10.48550/ARXIV.2205.13876. URL: https://arxiv.org/abs/2205.13876.

[60] B. J. Park et al. "Development of ultra-pure NaI(Tl) detectors for the COSINE-200 experiment". In: *The European Physical Journal C* 80.9 (Sept. 2020). DOI: 10.1140/epjc/s10052-020-8386-8.

[61] K Fushimi et al. "Development of highly radiopure NaI(Tl) scintillator for PICOLON dark matter search project". In: *Progress of Theoretical and Experimental Physics* 2021.4 (Feb. 2021). 043F01. ISSN: 2050-3911. DOI: 10.1093/ptep/ptab020. eprint: https://academic.oup.com/ptep/article-pdf/2021/4/043F01/37807808/ptab020.pdf. URL: https://doi.org/10.1093/ptep/ptab020.

[62] R. Bernabei et al. "Particle Dark Matter and DAMA/LIBRA". In: *AIP Conf. Proc.* 1223.1 (2010), pp. 50–59. DOI: 10.1063/1.3395996. arXiv: 0912.0660 [astro-ph.GA].

[63] M. Antonello et al. "Monte Carlo simulation of the SABRE PoP background". In: *Astropart. Phys.* 106 (2019), pp. 1–9. DOI: 10.1016/j.astropartphys.2018.10.005.

[64] E. Barberio et al. *Simulation of the SABRE South experiment and background characterization*. 2022. URL: https://arxiv.org/abs/2205.13849.

[65] M.R. Anderson et al. "Development, characterisation, and deployment of the SNO+ liquid scintillator". In: *Journal of Instrumentation* 16.05 (May 2021), P05009. DOI: 10.1088/1748-0221/16/05/p05009. URL: https://doi.org/10.1088%5C%2F1748-0221%5C%2F16%5C%2F05%5C%2Fp05009.

[66] Mohan Li et al. "Separation of Scintillation and Cherenkov Lights in Linear Alkyl Benzene". In: *Nuclear Instruments and Methods in Physics Research Section A: Accelerators, Spectrometers, Detectors and Associated Equipment* 830 (Nov. 2015). DOI: 10.1016/j.nima.2016.05.132.

[67] Y. Zhang et al. "A complete optical model for liquid-scintillator detectors". In: *Nuclear Instruments and Methods in Physics Research Section A: Accelerators, Spectrometers, Detectors and Associated Equipment* 967 (2020), p. 163860. ISSN: 0168-9002. DOI: https://doi.org/10.1016/j.nima.2020.163860. URL: https://www.sciencedirect.com/science/article/pii/S0168900220303648.

[68] Hamamatsu photonics. *Large cathode area photomultiplier tubes*. 2019. URL: https://www.hamamatsu.com/content/dam/hamamatsu-photonics/sites/documents/99_SALES_LIBRARY/etd/LARGE_AREA_PMT_TPMH1376E.pdf.

[69] F. Calaprice et al. "High sensitivity characterization of an ultrahigh purity NaI(Tl) crystal scintillator with the SABRE proof-of-principle detector". In: *Phys. Rev. D* 104 (2 July 2021), p. L021302. URL: https://doi.org/10.1103/PhysRevD.104.L021302.

[70] S. Agostinelli et al. "Geant4 – a simulation toolkit". In: *Nucl. Instrum. Methods Phys. Res. A: Accel. Spectrom. Detect. Assoc. Equip.* 506.3 (2003), pp. 250–303. ISSN: 0168-9002. URL: https://doi.org/10.1016/S0168-9002(03)01368-8.

[71] J. Allison et al. "Geant4 developments and applications". In: *IEEE Trans. Nucl. Sci.* 53 (2006), p. 270. URL: https://doi.org/10.1109/TNS.2006.869826.

[72] J. Allison et al. "Recent developments in Geant4". In: *Nucl. Instrum. Methods Phys. Res. A: Accel. Spectrom. Detect. Assoc. Equip.* 835 (2016), pp. 186–225. ISSN: 0168-9002. URL: https://doi.org/10.1016/j.nima.2016.06.125.

[73] V.N. Ivanchenko et al. "Geant4 models for simulation of multiple scattering". In: *J. Phys. Conf. Ser.* 219 (2010), p. 032045. URL: https://doi.org/10.1088/1742-6596/219/3/032045.

[74] D. Cullen, J.H. Hubbell, and L. Kissel. *The Evaluated Photon Data Library*. Report UCRL-50400, vol. 6. 1997.

[75] Nuclear Energy Agency. "PENELOPE 2018: A code system for Monte Carlo simulation of electron and photon transport". In: *OECD Publishing* (2019), p. 420. URL: https://doi.org/10.1787/32da5043-en.

[76] I Coarasa et al. "Machine-learning techniques applied to three-year exposure of ANAIS112". In: *Journal of Physics: Conference Series* 2156.1 (Dec. 2021), p. 012036. DOI: 10.1088/1742-6596/2156/1/012036. URL: https://doi.org/10.1088%5C%2F1742-6596%5C%2F2156%5C%2F1%5C%2F012036.

[77] W. J. D. Melbourne, 0. Stanley, and M. J. Zurowski. *Photomultiplier characterisation and its impact on Background for SABRE South*. 14th Internation Conference on Identification of Dark Matter. July 2022.

[78] G. Heusser. "Low-radioactivity background techniques". In: *Ann. Rev. Nucl. Part. Sci.* 45 (1995), pp. 543–590. DOI: 10.1146/annurev.ns.45.120195.002551.

[79] D. S. Akerib et al. "The LUX-ZEPLIN (LZ) radioactivity and cleanliness control programs". In: *The European Physical Journal C* 80.11 (Nov. 2020). DOI: 10.1140/epjc/s10052-020-8420-x. URL: https://doi.org/10.1140%5C%2Fepjc%5C%2Fs10052-020-8420-x.

[80] H. v. Wartenberg. "Benetzung durch geschmolzene Salze". In: *Angewandte Chemie* 69.8 (1957), pp. 258–262. DOI: 10.1002/ange.19570690804.

[81] Burkhant Suerfu et al. *Growth of Ultra-high Purity NaI(Tl) Crystal for Dark Matter Searches*. Tech. rep. 2019. arXiv: 1910.03782v1.

[82] Atherton Seidell. *Solubilities of inorganic and organic compounds, a compilation of quantitative solubility data from the periodical literature*. D. Van Nostrand Company, 1919, p. 633.

[83] J. R. Johnson. "The direct synthesis and purification of sodium iodide". In: (1965).

[84] Cassidy Hubert. *Sodium Carbonate Crystallisation Sample Results*. Aug. 2015.

[85] Alexander Wright. *Private correspondence*. 2019.

[86] Greg Henson. *Private correspondence, SeaStar Chemicals*. 2019.

[87] Jo Wu. *Internal SABRE report*. Aug. 2018.

[88] Burkhant Suerfu, Frank Calaprice, and Michael Souza. "Zone Refining of Ultrahigh-Purity Sodium Iodide for Low-Background Detectors". In: *Physical Review Applied* 16.1 (July 2021). DOI: 10.1103/physrevapplied.16.014060. URL: https://doi.org/10.1103%5C%2Fphysrevapplied.16.014060.

[89] C. Ha et al. "First Direct Search for Inelastic Boosted Dark Matter with COSINE-100". In: *Phys. Rev. Lett.* 122 (13 Apr. 2019), p. 131802. DOI: 10.1103/PhysRevLett.122.131802. URL: https://link.aps.org/doi/10.1103/PhysRevLett.122.131802.

[90] P. Adhikari et al. "First Direct Detection Constraints on Planck-Scale Mass Dark Matter with Multiple-Scatter Signatures Using the DEAP-3600 Detector". In: *Phys. Rev. Lett.* 128 (1 Jan. 2022), p. 011801. DOI: 10.1103/PhysRevLett.128.011801. URL: https://link.aps.org/doi/10.1103/PhysRevLett.128.011801.

[91] C. Galbiati and K. McCarty. "Time and space reconstruction in optical, non-imaging, scintillator-based particle detectors". In: *Nuclear Instruments and Methods in Physics Research Section A: Accelerators, Spectrometers, Detectors and Associated Equipment*

568.2 (Dec. 2006), pp. 700–709. DOI: 10.1016/j.nima.2006.07.058. URL: https://doi.org/10.1016%5C%2Fj.nima.2006.07.058.

[92] Ziyuan Li et al. "Event vertex and time reconstruction in large-volume liquid scintillator detectors". In: *Nucl. Sci. Tech.* 32.5 (2021), p. 49. DOI: 10.1007/s41365-021-00885-z. arXiv: 2101.08901 [physics.ins-det].

[93] J. Aalbers et al. "DARWIN: towards the ultimate dark matter detector". In: *Journal of Cosmology and Astroparticle Physics* 2016.11 (Nov. 2016), pp. 017–017. DOI: 10.1088/1475-7516/2016/11/017. URL: https://doi.org/10.1088%5C%2F1475-7516%5C%2F2016%5C%2F11%5C%2F017.

[94] W.J.D. Melbourne, M.J. Zurowski, and N. Spinks. *SABRE Digitisation - DOOM (Digitisation Of Optical Monte carlo)*. Version 1.0. Sept. 2022. DOI: 10.5281/zenodo.7127418. URL: https://doi.org/10.5281/zenodo.7127418.

[95] E.H. Bellamy et al. "Absolute calibration and monitoring of a spectrometric channel using a photomultiplier". In: *Nuclear Instruments and Methods in Physics Research Section A: Accelerators, Spectrometers, Detectors and Associated Equipment* 339.3 (1994), pp. 468–476. ISSN: 0168-9002. DOI: https://doi.org/10.1016/0168-9002(94)90183-X. URL: https://www.sciencedirect.com/science/article/pii/016890029490183X.

[96] G. F. Knoll. *Radiation Detection and Measurement*. Wiley, 2000.

[97] Geant4 Collaboration. *Geant4: Guide For Physics Lists, Release 10.7*. 2020. URL: https://geant4-userdoc.web.cern.ch/UsersGuides/PhysicsListGuide.

[98] Hamamatsu photonics. *Photomultiplier tubes and photomultiplier assemblies R11265U series/H11934 series*. 2019. URL: https://www.hamamatsu.com/content/dam/hamamatsu-photonics/sites/documents/99_SALES_LIBRARY/etd/R11265U_H11934_TPMH1336E.pdf.

[99] XIA LLC. *Pixie-16 User Manual*. 2019. URL: https://docs.nscl.msu.edu/daq/newsite/pixie16/Pixie16_UserManual.pdf.

[100] Madeleine J. Zurowski, Elisabetta Barberio, and Giorgio Busoni. "Inelastic Dark Matter and the SABRE experiment". In: *Journal of Cosmology and Astroparticle Physics* 2020.12 (Dec. 2020), p. 014. DOI: 10.1088/1475-7516/2020/12/014. URL: https://dx.doi.org/10.1088/1475-7516/2020/12/014.

[101] M.J. Zurowski and E. Barberio. "Influence of NaI background and mass on testing the DAMA modulation". In: *Eur. Phys. J. C* 82 (Dec. 2022), p. 1122. URL: https://doi.org/10.1140/epjc/s10052-022-11062-w.

[102] A. Liam Fitzpatrick et al. "The Effective Field Theory of Dark Matter Direct Detection". In: *JCAP* 1302 (2013), p. 004. DOI: 10.1088/1475-7516/2013/02/004. arXiv: 1203.3542 [hep-ph].

[103] Nikhil Anand, A. Liam Fitzpatrick, and W. C. Haxton. "Weakly interacting massive particle-nucleus elastic scattering response". In: *Phys. Rev.* C89.6 (2014), p. 065501. DOI: 10.1103/PhysRevC.89.065501. arXiv: 1308.6288 [hep-ph].

[104] Marco Cirelli, Eugenio Del Nobile, and Paolo Panci. "Tools for model-independent bounds in direct dark matter searches". In: *JCAP* 1310 (2013), p. 019. DOI: 10.1088/1475-7516/2013/10/019. arXiv: 1307.5955 [hep-ph].

[105] Sunghyun Kang, S. Scopel, and Gaurav Tomar. "Probing DAMA/LIBRA data in the full parameter space of WIMP effective models of inelastic scattering". In: *Phys. Rev.*

D99.10 (2019), p. 103019. DOI: 10.1103/PhysRevD.99.103019. arXiv: 1902.09121 [hep-ph].

[106] C. Patrignani et al. "Review of Particle Physics". In: *Chin. Phys.* C40.10 (2016), p. 100001. DOI: 10.1088/1674-1137/40/10/100001.

[107] Gaurav Tomar et al. "Is a WIMP explanation of the DAMA modulation effect still viable?" In: *16th International Conference on Topics in Astroparticle and Underground Physics (TAUP 2019) Toyama, Japan, September 9-13, 2019*. 2019. arXiv: 1911.12601 [hep-ph].

[108] Lina Necib, Mariangela Lisanti, and Vasily Belokurov. "Inferred Evidence For Dark Matter Kinematic Substructure with SDSS-Gaia". In: (2018). DOI: 10.3847/1538-4357/ab095b. arXiv: 1807.02519 [astro-ph.GA].

[109] Ciaran A. J. O'Hare et al. "Dark matter hurricane: Measuring the S1 stream with dark matter detectors". In: *Phys. Rev.* D98.10 (2018), p. 103006. DOI: 10.1103/PhysRevD.98.103006. arXiv: 1807.09004 [astro-ph.CO].

[110] Grace E. Lawrence et al. *Gusts in the Headwind: Uncertainties in Direct Dark Matter Detection*. 2022. DOI: 10.48550/ARXIV.2207.07644. URL: https://arxiv.org/abs/2207.07644.

[111] Helmer H. Koppelman et al. "Characterization and history of the Helmi streams with Gaia DR2". In: *Astron. Astrophys.* 625, A5 (May 2019), A5. DOI: 10.1051/0004-6361/201834769. arXiv: 1812.00846 [astro-ph.GA].

[112] G. C. Myeong et al. "Evidence for two early accretion events that built the Milky Way stellar halo". In: *Mon. Not. Roy. Astron. Soc.* 488.1 (Sept. 2019), pp. 1235–1247. DOI: 10.1093/mnras/stz1770. arXiv: 1904.03185 [astro-ph.GA].

[113] Amina Helmi et al. "The merger that led to the formation of the Milky Way's inner stellar halo and thick disk". In: *Nature* 563.7729 (Oct. 2018), pp. 85–88. DOI: 10.1038/s41586-018-0625-x. arXiv: 1806.06038 [astro-ph.GA].

[114] H.W. Joo et al. "Quenching factor measurement for NaI(Tl) scintillation crystal". In: *Astroparticle Physics* 108 (2019), pp. 50–56. ISSN: 0927-6505. DOI: https://doi.org/10.1016/j.astropartphys.2019.01.001. URL: https://www.sciencedirect.com/science/article/pii/S0927650518302561.

[115] J. D. Lewin and P. F. Smith. "Review of mathematics, numerical factors, and corrections for dark matter experiments based on elastic nuclear recoil". In: *Astropart. Phys.* 6 (1996), pp. 87–112. DOI: 10.1016/S0927-6505(96)00047-3.

[116] L. J. Bignell, I. Mahmood, et al. *Quenching factor measurements of sodium nuclear recoils in NaI:Tl determined by spectrum fitting*. preprint. 2021. arXiv: 2102.02833 [physics.ins-det].

[117] Jingke Xu et al. "Scintillation efficiency measurement of Na recoils in NaI(Tl) below the DAMA/LIBRA energy threshold". In: *Physical Review C* 92.1 (2015). ISSN: 1089-490X. DOI: 10.1103/physrevc.92.015807. URL: http://dx.doi.org/10.1103/PhysRevC.92.015807.

[118] Tyana Stiegler et al. *A study of the NaI(Tl) detector response to low energy nuclear recoils and a measurement of the quenching factor in NaI(Tl)*. preprint. 2017. arXiv: 1706.07494 [physics.ins-det].

[119] D. Cintas et al. "Quenching Factor consistency across several NaI(Tl) crystals". In: *Journal of Physics: Conference Series* 2156.1 (Dec. 2021), p. 012065. DOI: 10.1088/

1742-6596/2156/1/012065. URL: https://doi.org/10.1088%5C%2F1742-6596%5C%2F2156%5C%2F1%5C%2F012065.

[120] R. Bernabei et al. "Dark Matter search". In: (2003). DOI: 10.48550/ARXIV.ASTRO-PH/0307403. URL: https://arxiv.org/abs/astro-ph/0307403.

[121] D.R. Tovey et al. "Measurement of scintillation efficiencies and pulse-shapes for nuclear recoils in NaI(Tl) and CaF2(Eu) at low energies for dark matter experiments". In: *Physics Letters B* 433.1 (1998), pp. 150–155. ISSN: 0370-2693. DOI: https://doi.org/10.1016/S0370-2693(98)00643-1. URL: https://www.sciencedirect.com/science/article/pii/S0370269398006431.

[122] "Pulse shape discrimination and dark matter search with NaI(Tl) scintillator". In: *Astroparticle Physics* 11.3 (1999), pp. 287–302. ISSN: 0927-6505. DOI: https://doi.org/10.1016/S0927-6505(99)00004-3. URL: https://www.sciencedirect.com/science/article/pii/S0927650599000043.

[123] M. J. Zurowski. *BASTET*. https://github.com/mjzurowski/bastet. 2022.

[124] Glen Cowan et al. "Asymptotic formulae for likelihood-based tests of new physics". In: *The European Physical Journal C* 71.2 (Feb. 2011). DOI: 10.1140/epjc/s10052-011-1554-0. URL: https://doi.org/10.1140%5C%2Fepjc%5C%2Fs10052-011-1554-0.

[125] P. Adhikari et al. "Constraints on dark matter-nucleon effective couplings in the presence of kinematically distinct halo substructures using the DEAP-3600 detector". In: *Physical Review D* 102.8 (Oct. 2020). DOI: 10.1103/physrevd.102.082001.

[126] G. Adhikari et al. "COSINE-100 and DAMA/LIBRA-phase2 in WIMP effective models". In: *Journal of Cosmology and Astroparticle Physics* 2019.06 (July 2019), pp. 048–048. DOI: 10.1088/1475-7516/2019/06/048. URL: https://doi.org/10.1088%5C%2F1475-7516%5C%2F2019%5C%2F06%5C%2F048.

[127] Y.J. Ko et al. "Comparison between DAMA/LIBRA and COSINE-100 in the light of quenching factors". In: *Journal of Cosmology and Astroparticle Physics* 2019.11 (Nov. 2019), pp. 008–008. DOI: 10.1088/1475-7516/2019/11/008. URL: https://doi.org/10.1088/1475-7516/2019/11/008.

[128] M. R. Bharadwaj. *A systematic study on the effects of Tl dopant contribution to quenching factor measurements in NaI crystals*. IDM Conference, 2022. 2022.

[129] G. Adhikari et al. "Initial Performance of the COSINE-100 Experiment". In: *Eur. Phys. J. C* 78.2 (2018), p. 107. DOI: 10.1140/epjc/s10052-018-5590-x. arXiv: 1710.05299 [physics.ins-det].

[130] J. Amaré et al. "Performance of ANAIS-112 experiment after the first year of data taking". In: *Eur. Phys. J. C* 79.3 (2019), p. 228. DOI: 10.1140/epjc/s10052-019-6697-4. arXiv: 1812.01472 [astro-ph.IM].

[131] "An experiment to search for dark-matter interactions using sodium iodide detectors". In: *Nature* 564.7734 (2018), pp. 83–86. ISSN: 1476-4687. DOI: 10.1038/s41586-018-0739-1. URL: http://dx.doi.org/10.1038/s41586-018-0739-1.

[132] I. Coarasa et al. "ANAIS-112 sensitivity in the search for dark matter annual modulation". In: *The European Physical Journal C* 79.3 (Mar. 2019). DOI: 10.1140/epjc/s10052-019-6733-4. URL: https://doi.org/10.1140%5C%2Fepjc%5C%2Fs10052-019-6733-4.

[133] G. Adhikari and et al. "Search for a Dark Matter-Induced Annual Modulation Signal in NaI(Tl) with the COSINE-100 Experiment". In: *Physical Review Letters* 123.3

(2019). DOI: 10.1103/physrevlett.123.031302. URL: http://dx.doi.org/10.1103/PhysRevLett.123.031302.

[134] G. Adhikari and et al. *Lowering the energy threshold in COSINE-100 dark matter searches*. preprint. 2020. arXiv: 2005.13784 [physics.ins-det].

[135] F. James. "MINUIT Function Minimization and Error Analysis: Reference Manual Version 94.1". In: (1994).

[136] N. J. Spinks et al. "Pulse Shape Discrimination of low-energy nuclear and electron recoils for improved particle identification in NaI:Tl". In: (May 2022). arXiv: 2205.08723 [physics.ins-det].

[137] D. Baxter et al. "Recommended conventions for reporting results from direct dark matter searches". In: *The European Physical Journal C* 81.10 (Oct. 2021). DOI: 10.1140/epjc/s10052-021-09655-y. URL: https://doi.org/10.1140%5C%2Fepjc%5C%2Fs10052-021-09655-y.

[138] Alejandro Ibarra and Andreas Rappelt. "Optimized velocity distributions for direct dark matter detection". In: *Journal of Cosmology and Astroparticle Physics* 2017.08 (Aug. 2017), p. 039. DOI: 10.1088/1475-7516/2017/08/039. URL: https://dx.doi.org/10.1088/1475-7516/2017/08/039.

[139] Riccardo Catena et al. "Halo-independent comparison of direct detection experiments in the effective theory of dark matter-nucleon interactions". In: *Journal of Cosmology and Astroparticle Physics* 2018.07 (July 2018), pp. 028–028. DOI: 10.1088/1475-7516/2018/07/028.

[140] Felix Kahlhoefer et al. "Model-independent comparison of annual modulation and total rate with direct detection experiments". In: *Journal of Cosmology and Astroparticle Physics* 2018.05 (May 2018), pp. 074–074. DOI: 10.1088/1475-7516/2018/05/074.

[141] N. Wyn Evans, Ciaran A. J. O'Hare, and Christopher McCabe. *SHM^{++}: A Refinement of the Standard Halo Model for Dark Matter Searches in Light of the Gaia Sausage*. 2018. DOI: 10.48550/ARXIV.1810.11468. URL: https://arxiv.org/abs/1810.11468.

[142] Ciaran A. J. O'Hare et al. "Velocity substructure from Gaiaand direct searches for dark matter". In: *Physical Review D* 101.2 (Jan. 2020). DOI: 10.1103/physrevd.101.023006. URL: https://doi.org/10.1103%5C%2Fphysrevd.101.023006.